

Article

# Ghost Fringe Suppression by Modifying the f-Number of the Diverger Lens for the Interferometric Measurement of Catadioptric Telescopes

Yi-Kai Huang <sup>1,2</sup>  and Cheng-Huan Chen <sup>1,\*</sup>

<sup>1</sup> Department of Photonics, College of Electrical and Computer Engineering, National Yang Ming Chiao Tung University, 1001 University Road, Hsinchu 310403, Taiwan; kai80108@gmail.com

<sup>2</sup> Optical Payload Division, Taiwan Space Agency, 8F, 9 Prosperity 1st Road, Hsinchu Science Park, Hsinchu 310403, Taiwan

\* Correspondence: chhuchen@nycu.edu.tw

**Abstract:** A high-precision catadioptric telescope such as a space-borne telescope is usually tested with interferometer to check the optical quality in assembly. The coarse and fine alignment of the telescope are mainly based on the information from the coordinate measuring machine and the fringe pattern of the interferometer, respectively. In addition, further fine-tuning can be achieved according to the variation in wavefront error and Zernike data. The issue is that the vast majority of the catadioptric telescopes contain plural lens surfaces which could produce unwanted ghost fringes, disturbing the wavefront measurement. Technically, off-axis installation to shift away ghost fringes from central interferogram could be acceptable in some cases. Nevertheless, in this paper, the source of ghost fringe in interferometric measurement for catadioptric telescopes is investigated with light path simulation, and a solution of reducing the f-number of the diverger lens is proposed to eliminate the ghost fringe disturbance. Both simulation and experimental results verify the effectiveness of the proposed concept.

**Keywords:** catadioptric telescope; interferometry; ghost fringes



**Citation:** Huang, Y.-K.; Chen, C.-H. Ghost Fringe Suppression by Modifying the f-Number of the Diverger Lens for the Interferometric Measurement of Catadioptric Telescopes. *Photonics* **2024**, *11*, 453. <https://doi.org/10.3390/photonics11050453>

Received: 26 March 2024

Revised: 3 May 2024

Accepted: 10 May 2024

Published: 11 May 2024



**Copyright:** © 2024 by the authors. Licensee MDPI, Basel, Switzerland. This article is an open access article distributed under the terms and conditions of the Creative Commons Attribution (CC BY) license (<https://creativecommons.org/licenses/by/4.0/>).

## 1. Introduction

Optical telescopes such as catadioptric and full-mirror-type systems are often applied in astronomical research, earth observation missions and deep space exploration. The ROCSAT-2 and Pleiades HR both served as successful earth observation satellites with a lifetime of more than 10 years; they featured the high-end catadioptric type and full-mirror-type systems with an aperture over 60 cm, respectively [1,2]. Recently, Canon Electronics Inc. has developed several low-cost micro-satellites equipped with the optical payload consisting of their own digital camera and a 40 cm diameter catadioptric telescope aiming at commercial earth observation applications [3]. The examples above show that the catadioptric telescope plays an important role in high-end and low-cost solutions for space telescopes.

In this paper, a catadioptric telescope was designed to conduct an earth observation mission in a 500–600 km altitude orbit and it could provide multi-spectral images with a 450–890 nm wavelength band. The catadioptric telescope is a circularly symmetric system and features easier fabrication and faster alignment compared to more advanced architectures such as the full-mirror off-axis system which usually replaces the corrector lens with a tertiary mirror. In order to meet the tight schedule of deploying a constellation of remote sensing satellites, the catadioptric telescope could be a decent candidate for the optical payload of the earth observation mission. The optical layout of the telescope is shown in Figure 1; it consists of a 40 cm diameter primary mirror (M1), a 14 cm diameter

secondary mirror (M2) and a 4-lens corrector module [4], where the color rays represent the light path of each field.

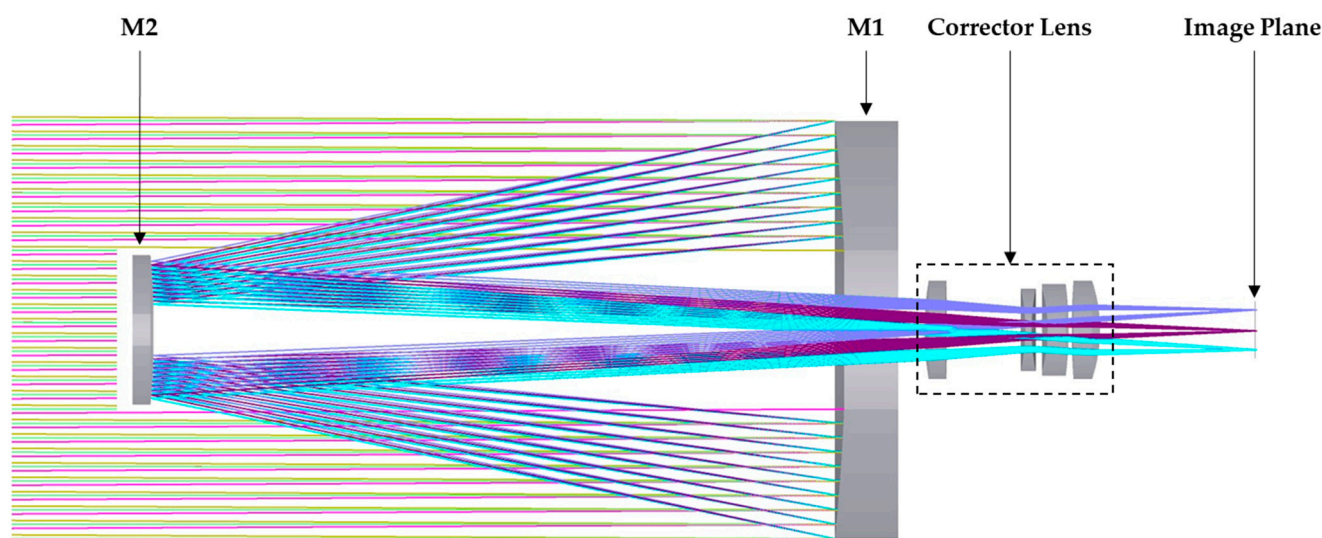


**Figure 1.** Optical layout and light path of catadioptric telescope.

Both mirrors are made of a low coefficient of thermal expansion (CTE) substrate with high-reflectance silver coating on their optical surfaces, and the lenses are made of fused silica with broad-band anti-reflective coating (reflectance less than 2%) on each surface. The alignment and assembly of the corrector lens are accomplished with an allocated maximum range of tilt and decenter error budgets less than  $\pm 60$  arcsec and  $\pm 75$   $\mu\text{m}$ , respectively.

The optical quality of the entire system is usually measured with an interferometer. Figure 2 shows the full light path of the double-pass interferometric measurement system of the catadioptric telescope with a Twyman–Green interferometer which adopts a spherical diverger lens with an  $f$ -number of 7. An auto collimation flat mirror with a clear aperture of 24 inches is employed to construct a double-pass architecture for the interferometric measurement. In addition, a pinhole array, consisting of five pinholes with a diameter of 1 mm, as illustrated in Figure 2, is used to define the measurement fields, including one on-axis field and four off-axis fields, and is placed on the image plane of the telescope.

A converging beam (He-Ne laser 632.8 nm), produced by the interferometer and the diverger lens, focuses onto the pinhole and then passes through the corrector to enter the telescope. After being reflected by M2 and M1 sequentially, it becomes collimatedly incident onto the auto collimation flat mirror. The reflected beam from the auto collimation flat mirror then returns to the telescope and interferometer by following the original light path. This to and fro route becomes the so-called double-pass light path. Finally, an interferogram can be obtained with the superposition of the return beam from the telescope and the reference beam from the reference mirror on the detector of the interferometer.

Before executing the interferometry, a sequence of mechanical alignments with a coordinate measuring machine (CMM) is conducted which will eventually leave an alignment error at the micrometer scale. The interferometry is then used for fine-tuning the position of optical components by monitoring the wavefront error (WFE). The final system wavefront data will be acquired in multiple average based on the standard deviation to eliminate the influence of random disturbances such as vibration and turbulence.

The full-field interferograms and corresponding WFE maps are shown in Figures 3 and 4, respectively. The interferogram shows a coarse fringe from the overall telescope optics and several fine fringes which constitute unwanted disturbance called ghost fringe. Consequently, the WFE map in Figure 4 shows broken patches where the ghost fringes are located, and those broken patches highly disturb the evaluation of the wavefront error. The other four off-axis fields present nominal WFE maps without ghost fringe disturbance.

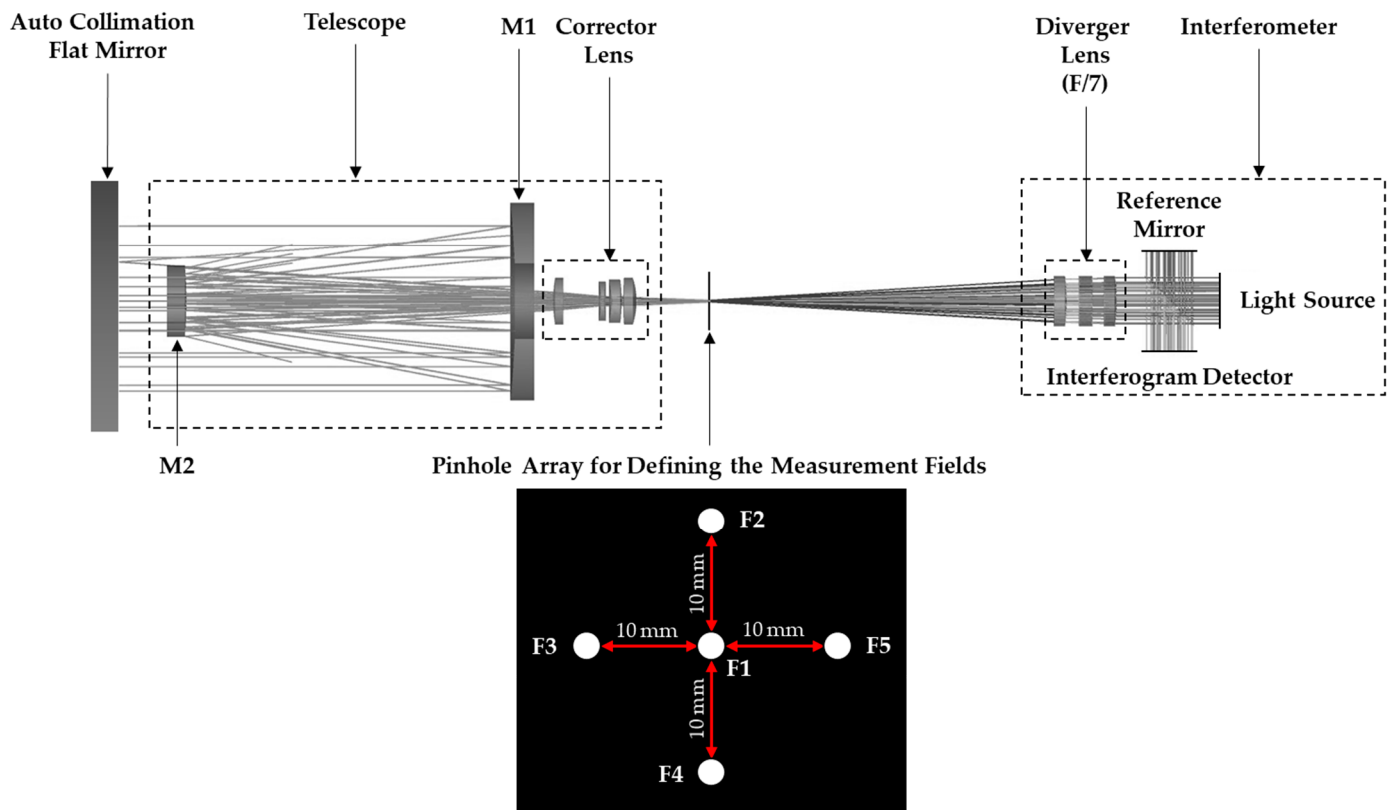


Figure 2. Interferometric measurement setup and light path for catadioptric telescope.

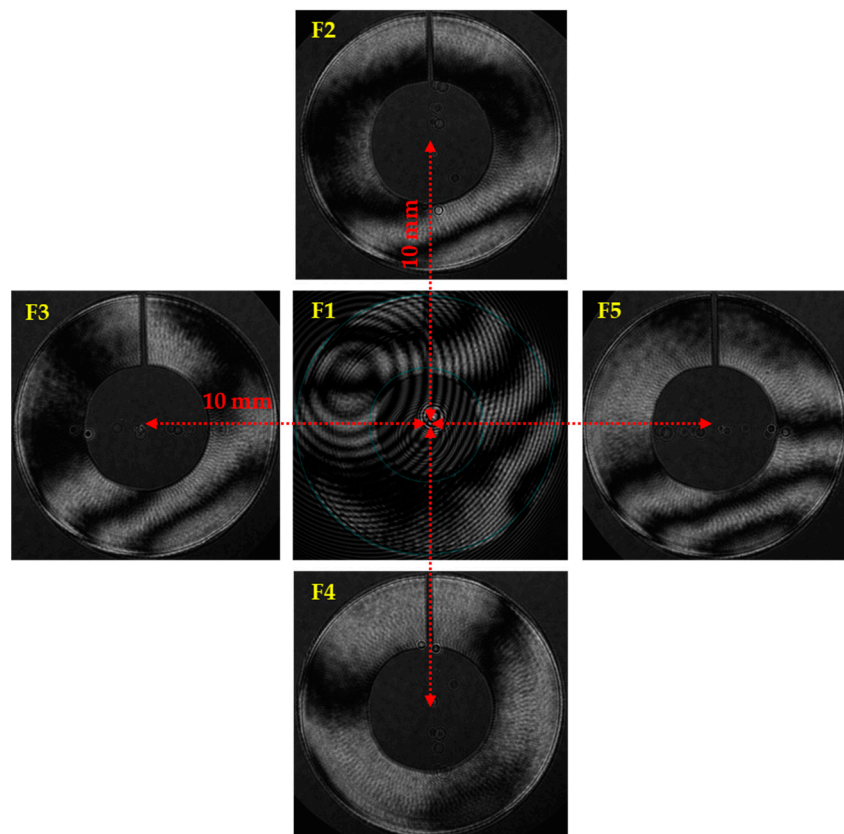
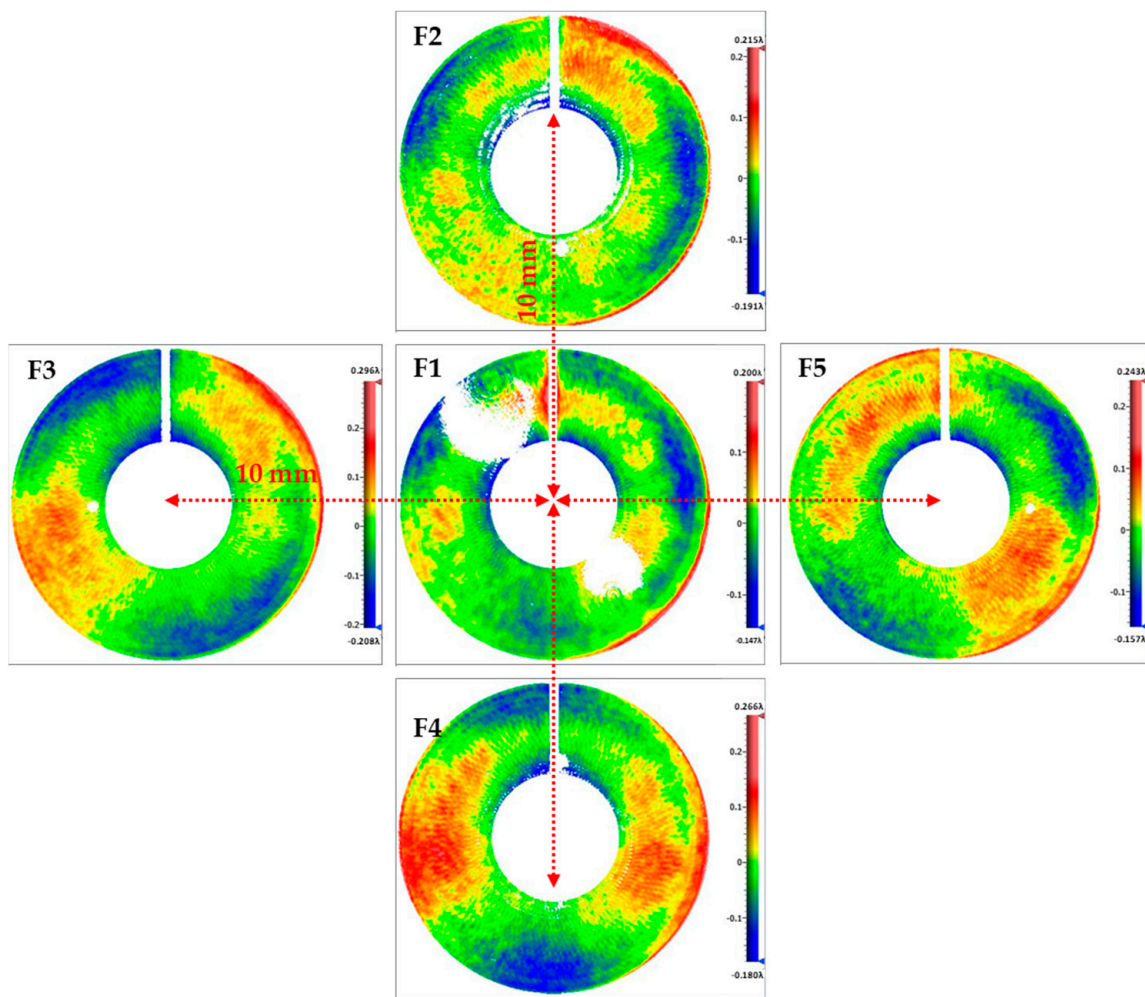


Figure 3. Full-field interferograms of one on-axis field (F1) and four off-axis fields (F2–F5).



**Figure 4.** Full-field WFE maps of one on-axis field (F1) and four off-axis fields (F2–F5).

Technically, the ghost fringes can be shifted away from the on-axis interferogram with a slight off-axis installation of the setup shown in Figure 2, and this approach can be acceptable in cases where the full-field WFE results satisfy the requirement with good aberration symmetry, but it is not applicable in general. Ghost images are classified according to the number of reflections encountered in the ghost ray path [5]. In imaging applications, ghost images could cause contrast reduction and veil parts of the image [6]. The light reaching the nominal image plane could also degrade the image quality [7]. Too many concentrated ghosts can disqualify a candidate lens design, equivalent to the effect of aberration [8]. The intensity of a ghost image is proportional to the product of the reflection coefficient of the coating on the refractive interfaces involved in the ghost light path and inversely proportional to the area of the ghost image [9]. In this paper, the source of the ghost fringe for the catadioptric telescope is investigated and the solutions to resolve the issue without off-axis installation are proposed and verified.

## 2. Source of Ghost Fringe in Catadioptric Telescope

In experiments, when a mask is located between the primary mirror and the corrector, blocking the laser beam from entering the mirrors, the ghost fringes still remain on the interferogram, as shown in Figure 5. This shows that the ghost fringe mainly comes from the corrector lens. When adjusting the position of the corrector, the ghost fringe shifts on the interferogram in accordance.

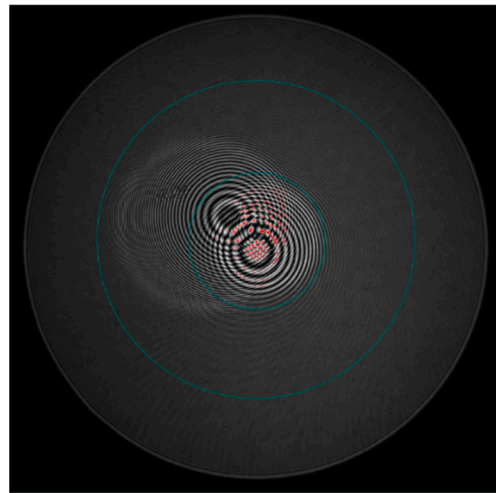


Figure 5. Interferogram of corrector module.

Theoretically, there should be an infinite number of ghost fringes. For practical engineering purposes, only the ones with sufficient intensity to disturb the correct reading of the original system fringe should be considered. Therefore, only the ghost light path with the first reflection from a refractive surface will be examined. As there are four lens elements in the corrector module, there should be a total of eight ghost light paths meeting this condition. However, to form a clear ghost fringe on the interferogram, the ghost light path should have a focus point close to that of the original system interferometric light path, i.e., the position of the pinhole shown in Figure 2. As a consequence, the most likely source of the ghost fringe come from the surfaces which are concave toward the pinhole, i.e., surface 1 of lens 1 (L1S1), L2S2, and L4S1, as illustrated in Figure 6, where the corrector module and the light path through it in Figure 1 are highlighted to show the labels of optical surfaces for the corrector.

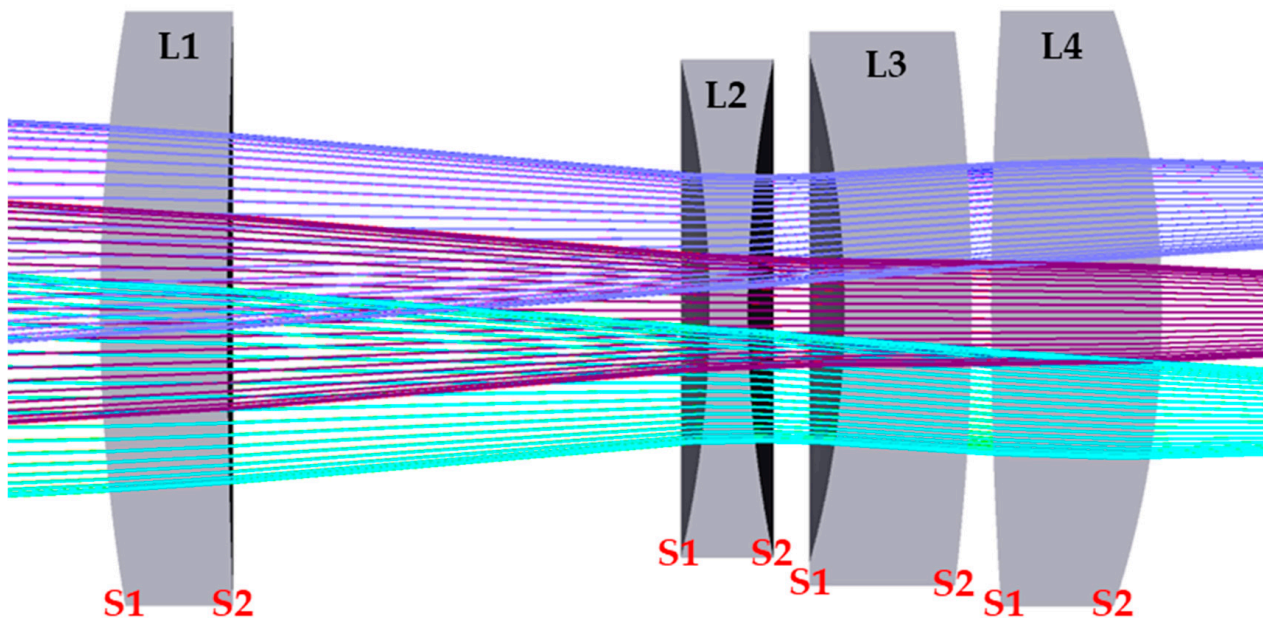
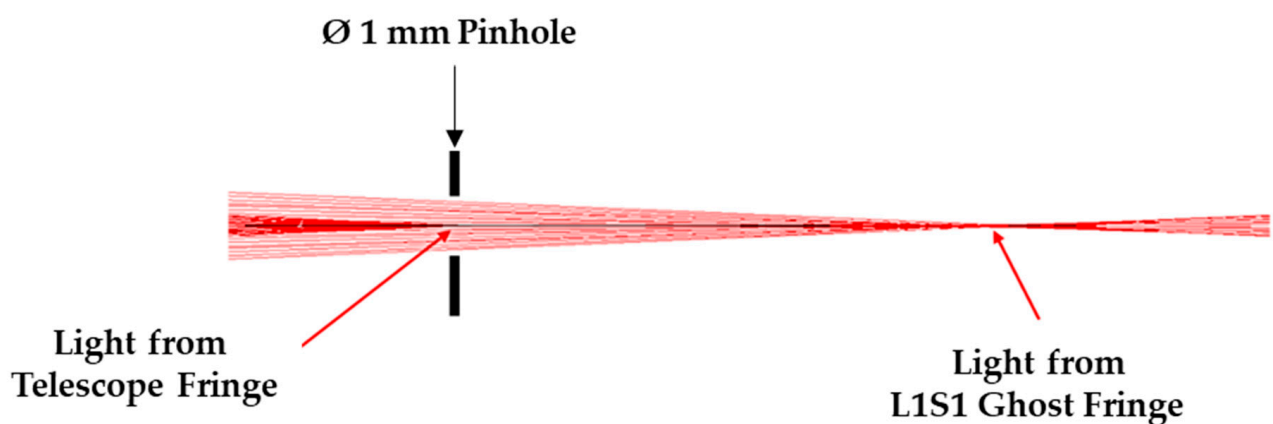


Figure 6. Labels of refractive surfaces for corrector module.

The distances between the center of curvature of those three surfaces and the pinhole are listed in Table 1. According to the table, the center of curvature of L1S1 is the one closest to the pinhole, and the corresponding ghost fringe could be the largest and strongest. Its light path through the pinhole is simulated and illustrated in Figure 7.

**Table 1.** Distance between pinhole and center of curvature of three surfaces.

| Surface | Distance (mm) |
|---------|---------------|
| Pinhole | 0             |
| L1S1    | −22.7         |
| L2S2    | 48.2          |
| L4S1    | −99.6         |



**Figure 7.** Light path of telescope fringe and L1S1 ghost fringe.

An alternative approach to get around the disturbance of ghost fringes is to tilt the corrector module such that the reflected ghost light is directed out of the path toward the detector or image plane [10]. To further confirm the source of the ghost fringe, the corrector module was tilted with respect to the center of curvature of the three surfaces listed in Table 1. For example, when tilting the corrector with respect to the center of curvature of L1S1, the corresponding ghost fringe from L1S1 will stay at its original position. Based on the abovementioned optical simulation and experimental results, it is confirmed that the largest ghost fringe is from L1S1, whereas the other two smaller ghost fringes are from L2S2 and L4S1.

### 3. Elimination of the Ghost Fringe

For eliminating the ghost fringes, several solutions have been proposed, including anti-reflection coating, polarization alteration, optical parameter manipulation, etc. The most direct way with minimum modification on the original optical system would be anti-reflection coating at the wavelength of the interferometer on the surfaces causing ghost fringes. Figure 8 shows the spectral reflectivity of the coating for L1S1, where new coating has been designed specially for anti-reflection at the 632.8 nm wavelength of the He-Ne laser, which is used as the light source in the interferometer. The interferogram of the corrector and the WFE of the whole telescope with nominal and new coating on L1S1 are shown in Figure 9, which indicates that the new coating is effective in eliminating the ghost fringe. Nevertheless, the modification is made only for accommodating interferometric measurements in the assembly process, which might not be an optimal design or might even cause side effects in real applications. This means that the approach is not a generic solution.

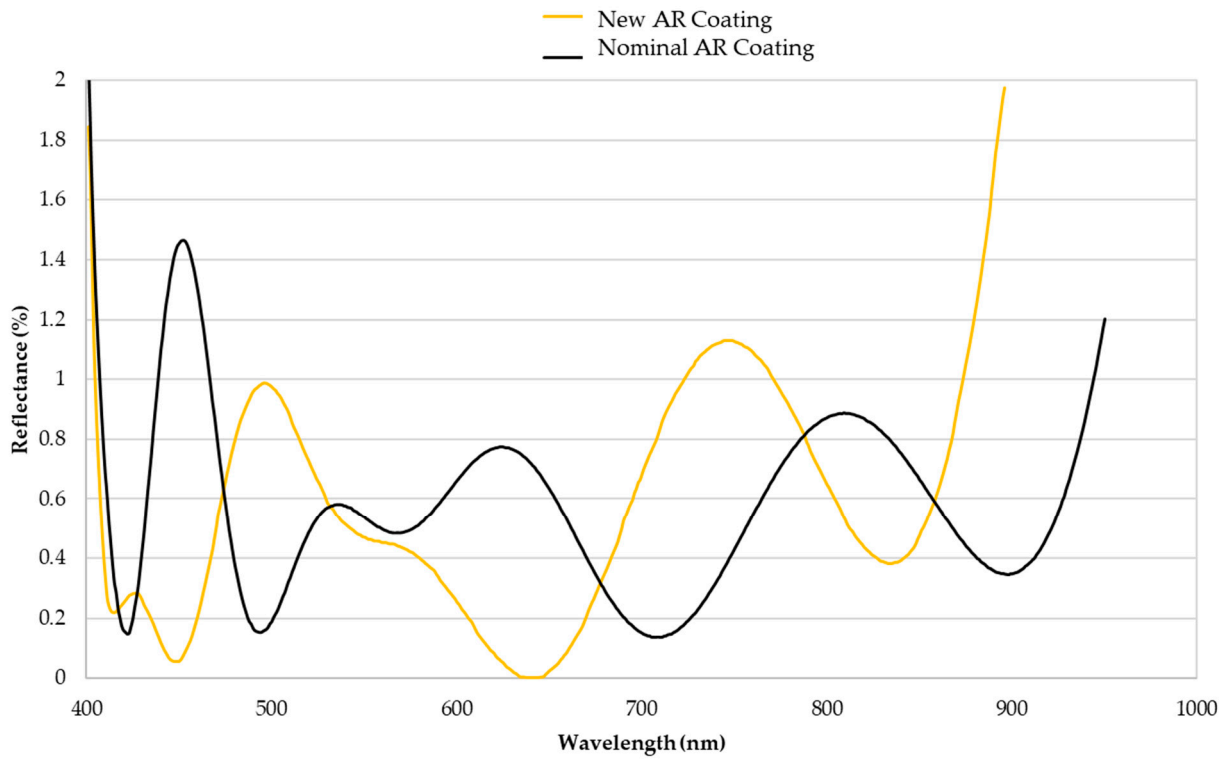


Figure 8. Spectral reflectance of L1S1 with nominal AR coating and new AR coating.

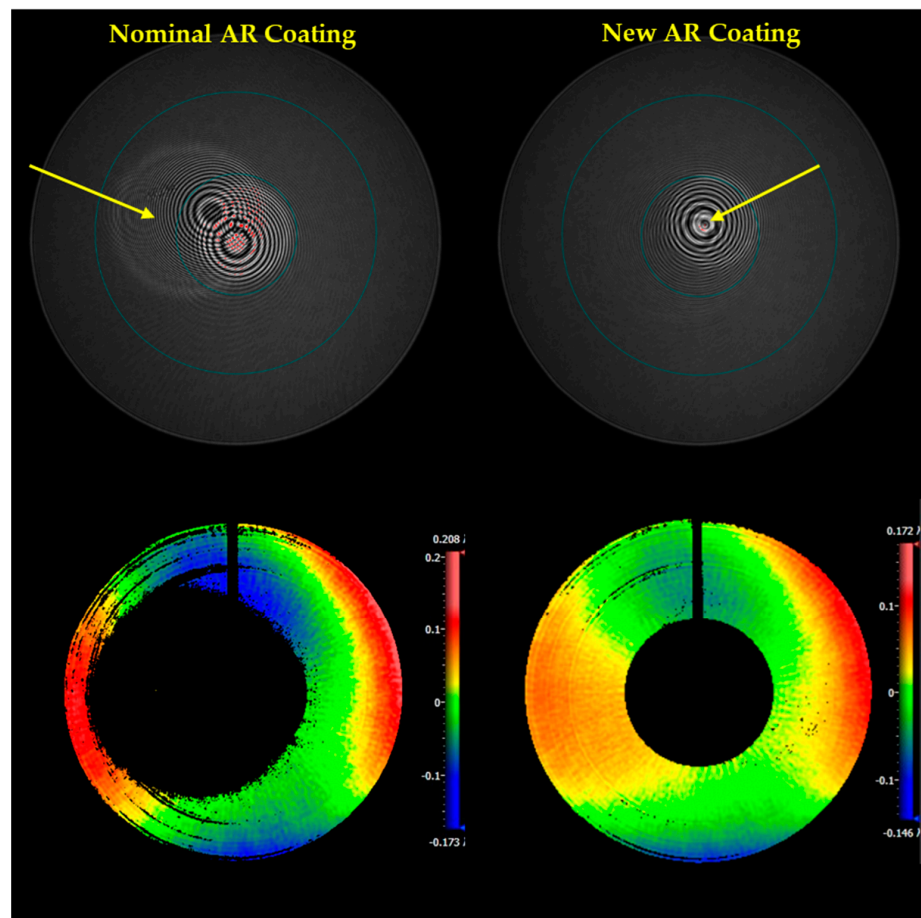
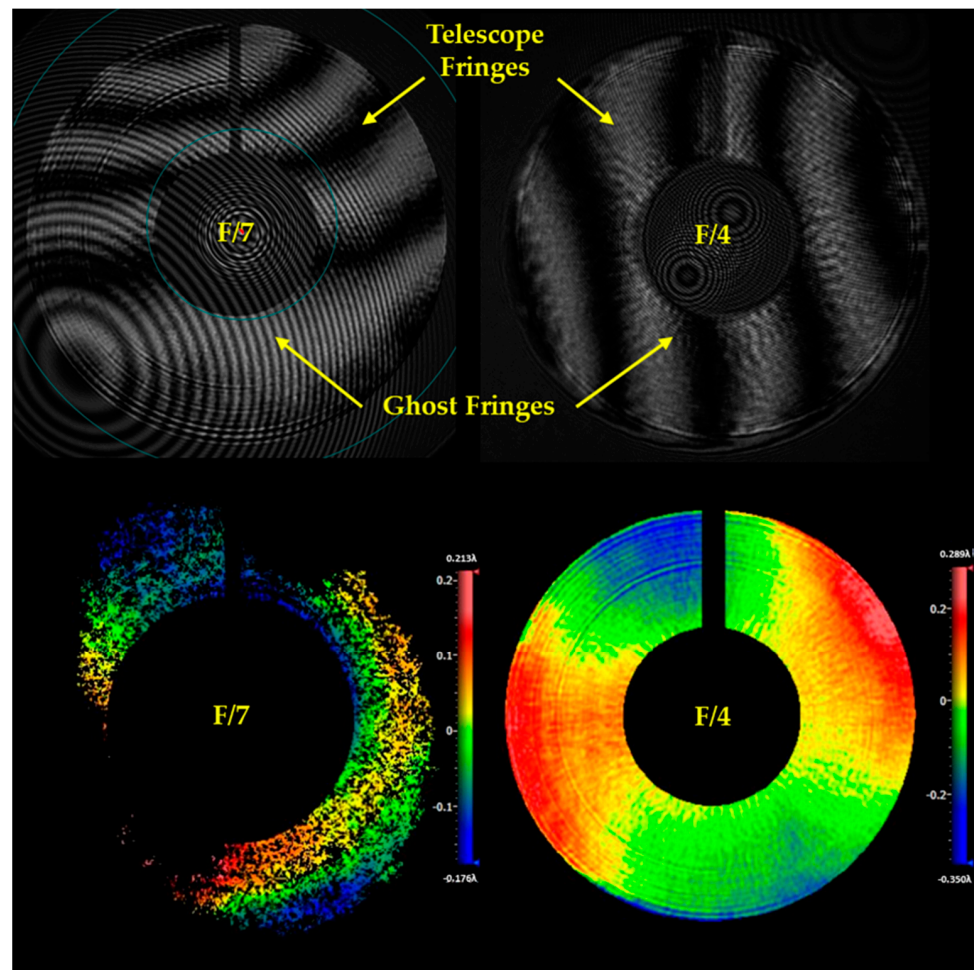


Figure 9. Cont.



**Figure 9.** Interferogram of corrector only and WFE map of telescope with nominal AR coating and new AR coating.

By examining the light path shown in Figure 7, reducing the size of the pinhole should be able to block more energy from the ghost light path while allowing through the desired light from the telescope, consequently reducing the relative contrast of the ghost fringe. However, the minimum pinhole size is normally determined by the feasibility of the optical alignment process. An alternative but equivalent modification would be to change the f-number of the diverger lens of the interferometer.

The analysis of the influence of the f-number on the ghost fringe was conducted with the non-sequential mode of Zemax [11,12] by calculating the contrast of coherent irradiance. An aberration-free module, consisting of three lens elements, was designed to act as the diverger lens in the interferometric light path, as shown in Figure 2. A 1 mm diameter pinhole with absorbing coating material was located at the image plane of the telescope. The whole interferometric system consisted of a diverger lens module, a reference mirror, a light source at 632.8 nm with  $1 \text{ w/cm}^2$  power, and an interferogram detector with  $1000 \times 1000$  pixels.

For the first configuration, perfect AR coating with 100% transmittance was applied to all surfaces of the corrector lens module to simulate the interferometric fringe of the whole telescope. The corresponding coherent irradiance on the interferogram and cross-sectional distribution are shown in Figure 10. The maximum value of coherent irradiance was calculated by averaging the top 100 data points and the result was  $0.0083 \text{ w/cm}^2$ .

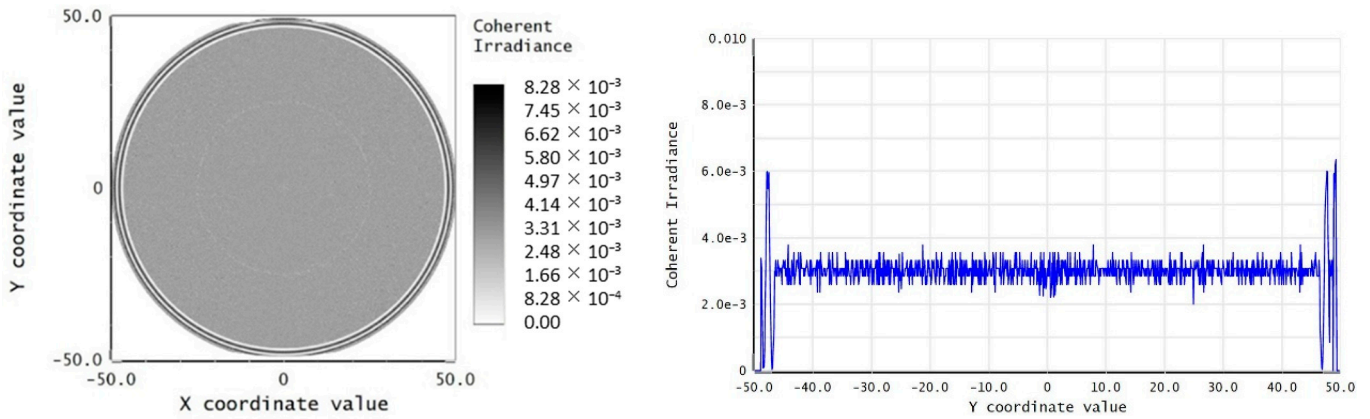


**Figure 10.** Coherent irradiance of interferogram and cross-sectional distribution for the whole telescope.

Secondly, in order to simulate only the ghost fringe from L1S1, the mirror surface was applied on L1S1, as shown in Figure 11. With this setup, the coherent irradiance purely from L1S1 could be obtained, as shown in Figure 12. The maximum value of coherent irradiance was 0.0106 w/cm<sup>2</sup>.

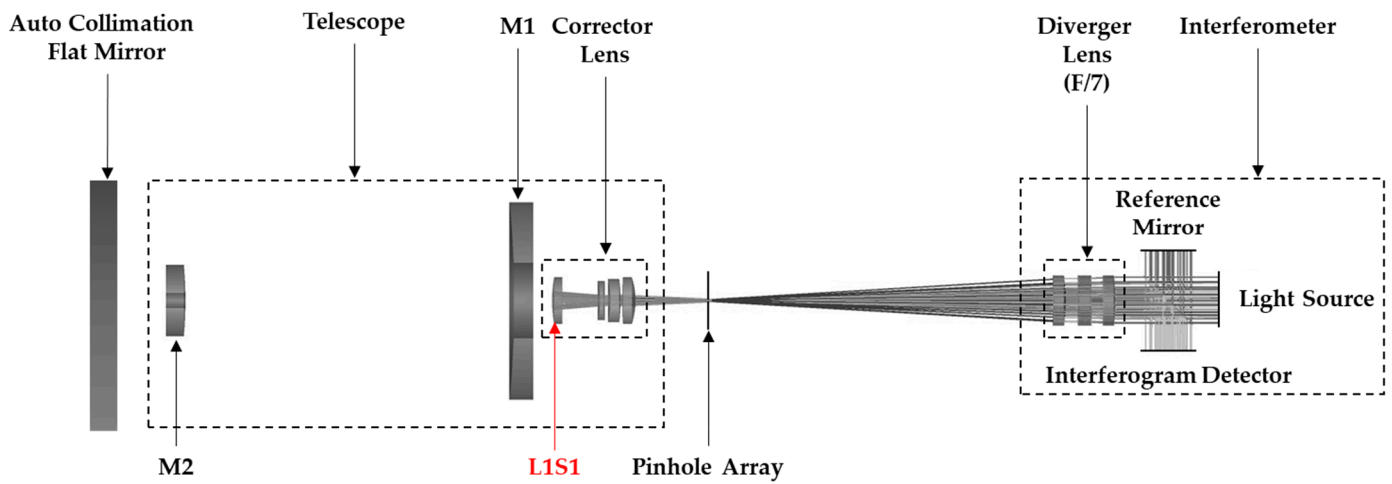


**Figure 11.** Interferometric light path of ghost fringe from L1S1.

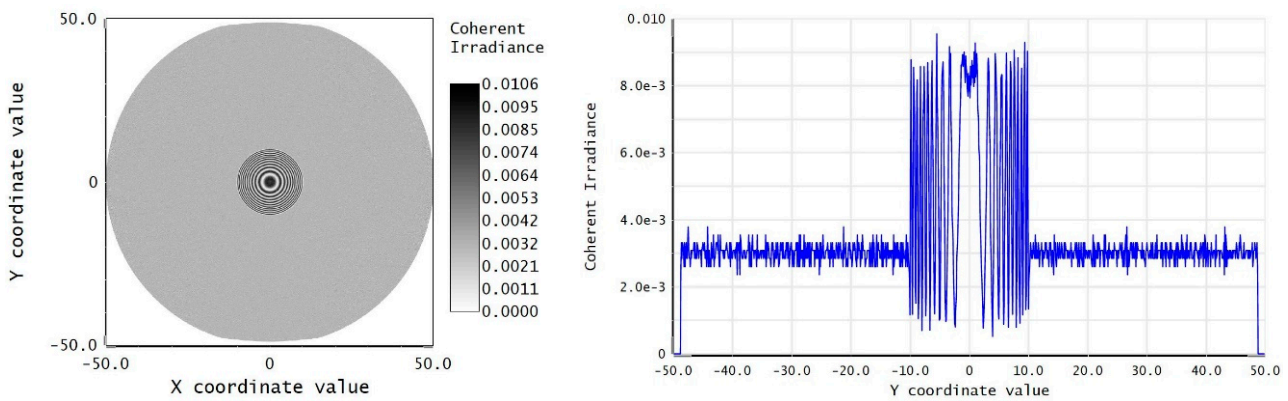


**Figure 12.** Coherent irradiance of interferogram and cross-sectional distribution for L1S1 ghost fringe only.

Finally, the superposition of the telescope fringe and the ghost fringe was simulated by applying 50% transmittance coating on L1S1. The gray scale graph of coherent irradiance

with both the original telescope fringe and the ghost fringe from L1S1 is shown in Figure 13. Based on this diagram, the contrast of the original fringe to the ghost fringe could be evaluated, which was around 60%.

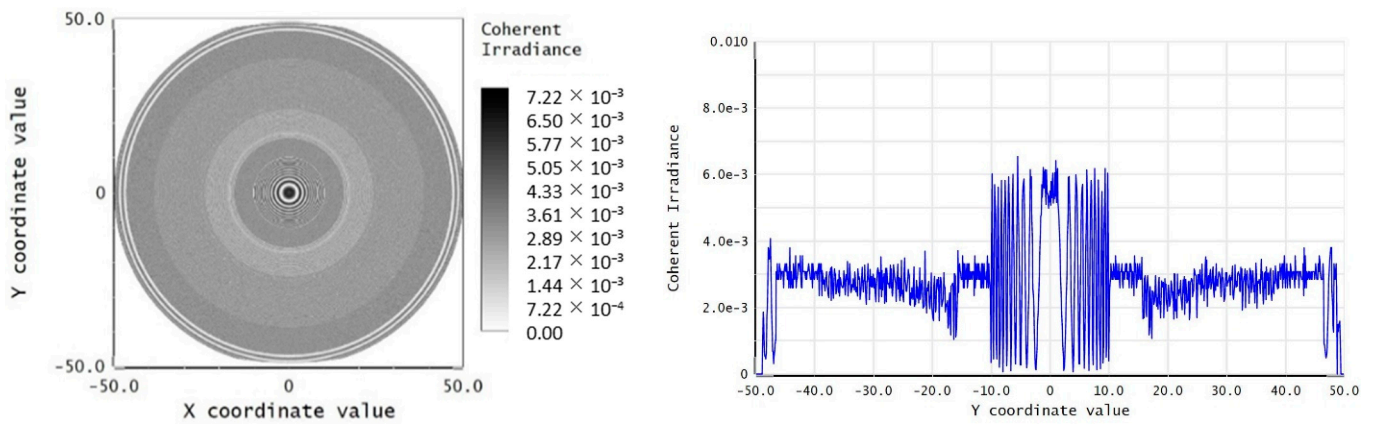


**Figure 13.** Coherent irradiance of interferogram and cross-sectional distribution for the superposition of telescope fringe and ghost fringe from L1S1.

A similar analysis can be performed for different f-numbers of the diverger lens module. Figure 14 shows the contrast of the telescope fringe to the ghost fringe with different f-numbers of the diverger lens module from F/7 to F/4. It indicates that the contrast increases with the reduction in f-number, and it exceeds 100%, i.e., the intensity of the telescope fringe surpass that of the ghost fringe from L1S1, at F/4 of the diverger lens. The comparison of the superposition fringe for F/7 and F/4 is shown in Table 2.

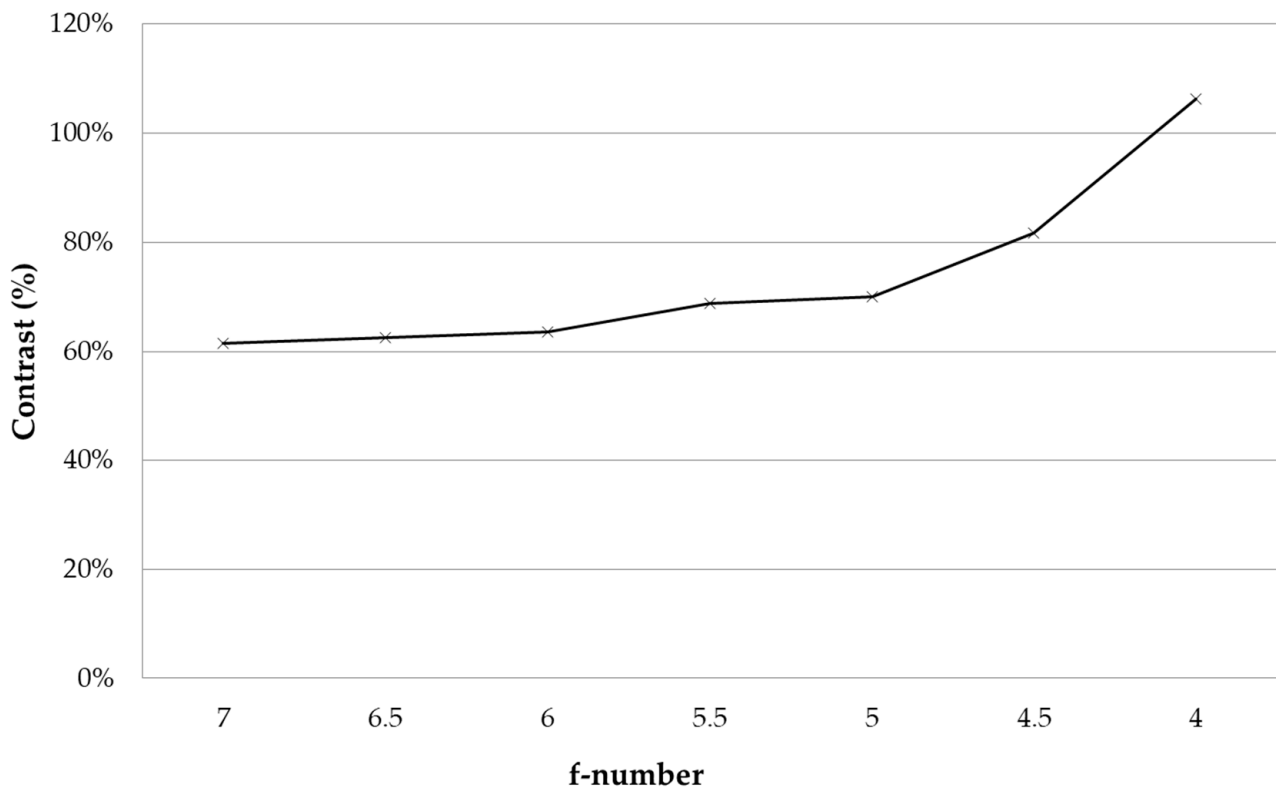
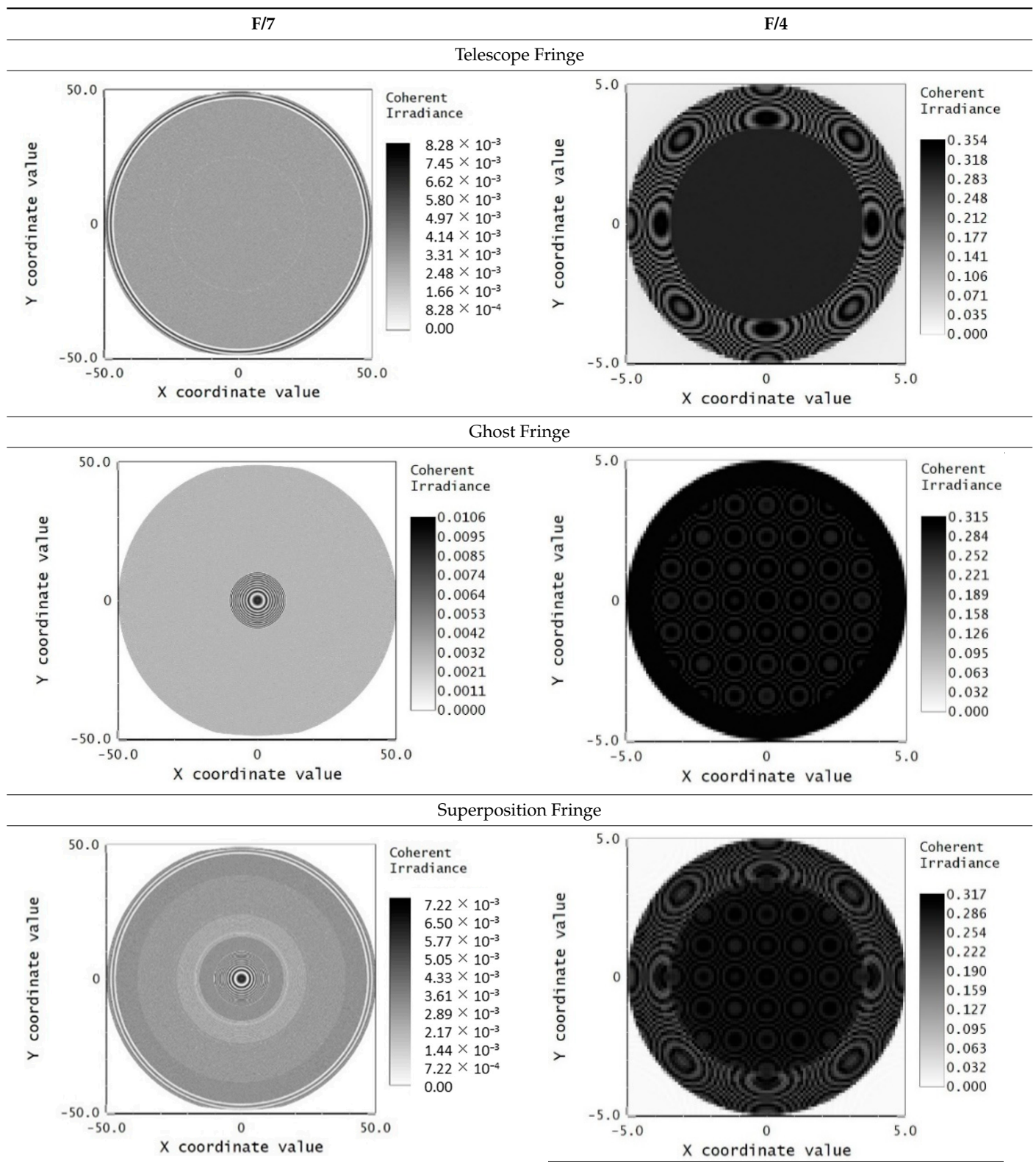


**Figure 14.** Contrast of telescope fringe to ghost fringe versus f-number of diverger lens module.

**Table 2.** Comparison of telescope fringe, ghost fringe and superposition fringe for F/7 and F/4.



#### 4. Experimental Results

Based on the simulation and analytical results with Zemax, the corresponding experiment was carried out for verification. For the spatial filter (pinhole) obscuration test, the size was changed from the original diameter of 1 mm to 0.3 mm, as shown in Figure 15, and the corresponding test result is shown in Figure 16. The light from the ghost fringe could be partially obscured by a 1 mm diameter pinhole but was largely obscured by a 0.3 mm diameter pinhole. The relative contrast of the telescope fringe to the ghost fringe could be increased, which is beneficial for the reconstruction of the WFE map with less data loss. However, the smaller the pinhole, the more time-consuming the alignment.

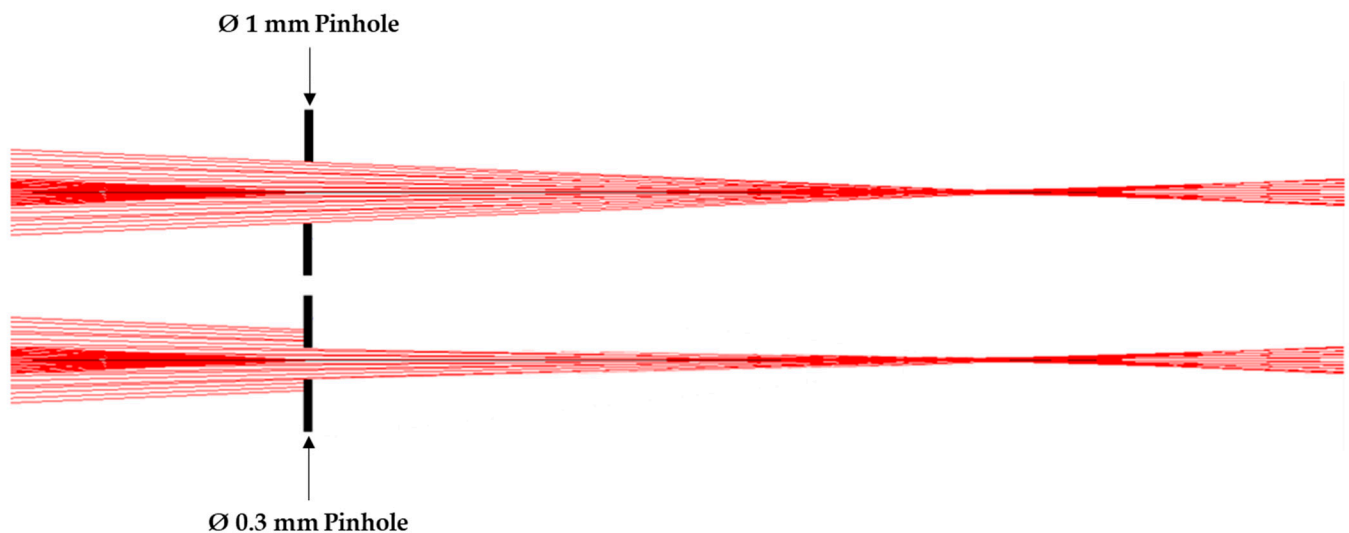


Figure 15. Light path through pinhole with different pinhole sizes.

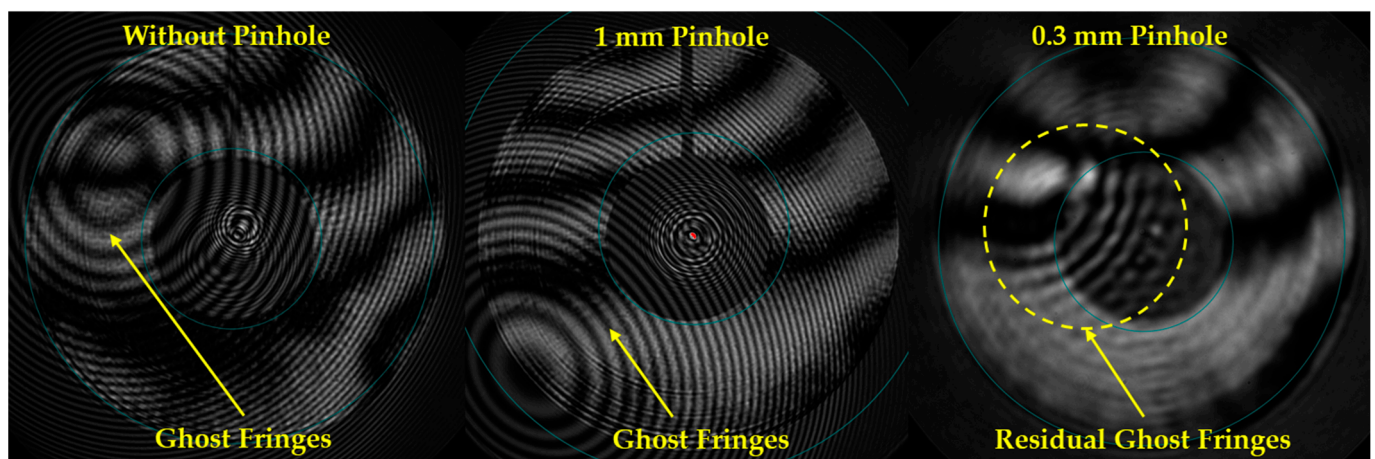


Figure 16. Interferogram of telescope without pinhole and with pinhole sizes of 1 mm and 0.3 mm.

The alternation is to reduce the f-number of the diverger lens while keeping the pinhole size at 1 mm. Figure 17 shows the interferogram and the WFE map of the telescope for the f-number of the diverger lens at F/4 and F/7. It indicates that a nearly perfect WFE map was obtained with F/4, which matched the desired improvement obtained in the simulation.

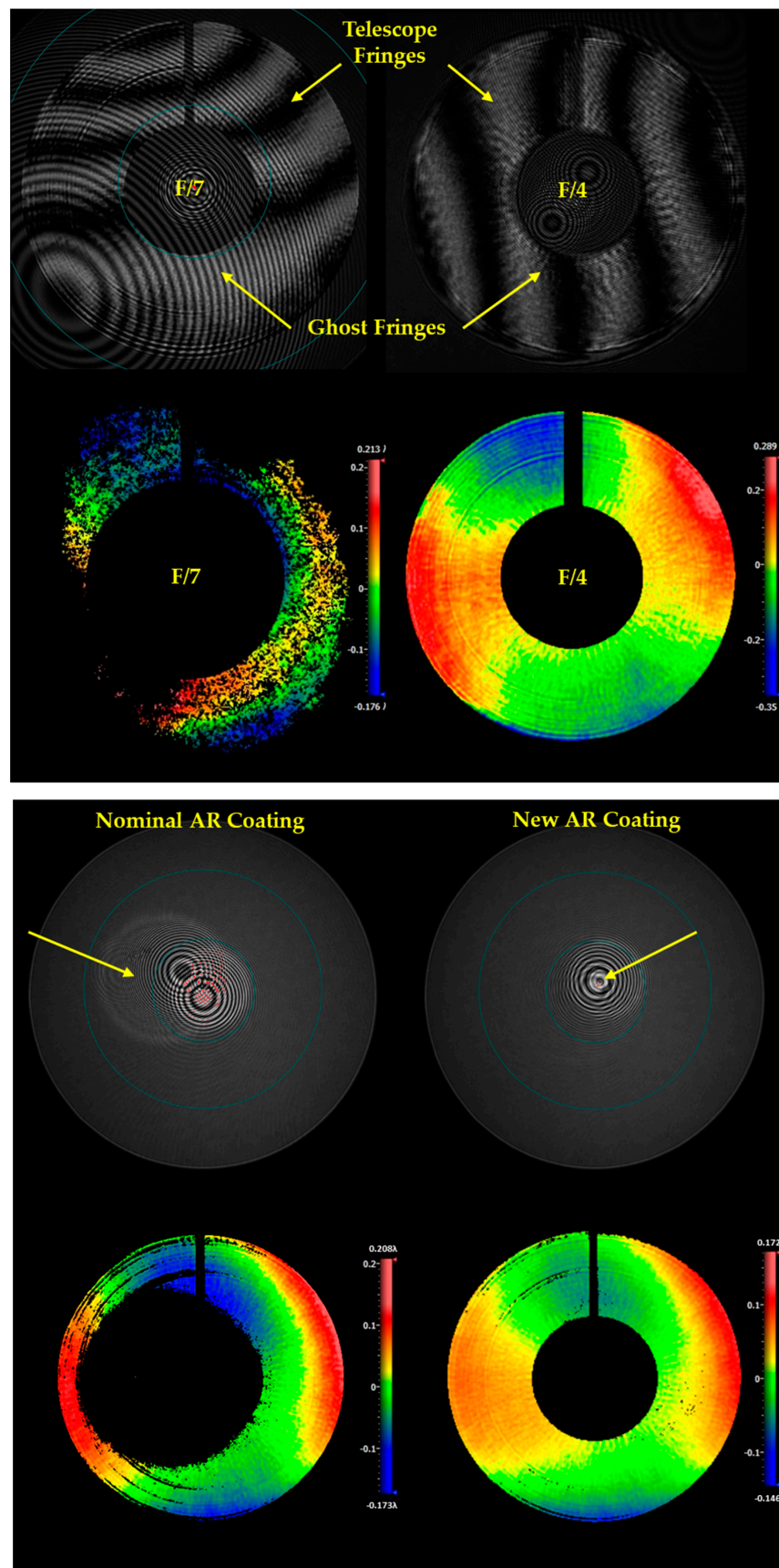


Figure 17. Interferogram and WFE map of telescope with f-number of diverger lens at F/4 and F/7.

## 5. Conclusions

High-quality catadioptric telescopes have been increasingly used in commercial applications in recent years. The fast assembly of this kind of telescopes, with various specifications to meet the launching schedule of satellites, has become a more important issue. The proposed approach was verified as an effective solution for the alignment of catadioptric telescopes without the disturbance from ghost fringes. Once a suitable  $f$ -number of the diverger lens is found, it can be used for the testing of the same batch. For the other batches with different specifications, the only part that needs to be changed in the whole interferometric test system is the diverger lens. Due to the fact that the solution is applied to the interferometer side, a similar concept can be applicable to all the other high-quality optical systems involving transmissive optical elements.

**Author Contributions:** Conceptualization, Y.-K.H.; methodology, Y.-K.H.; software, Y.-K.H.; validation, Y.-K.H.; formal analysis, Y.-K.H.; investigation, Y.-K.H.; data curation, Y.-K.H.; writing—original draft preparation, Y.-K.H.; writing—review and editing, C.-H.C.; visualization, Y.-K.H.; supervision, C.-H.C. All authors have read and agreed to the published version of the manuscript.

**Funding:** This research received no external funding.

**Institutional Review Board Statement:** Not applicable.

**Informed Consent Statement:** Not applicable.

**Data Availability Statement:** Data is unavailable due to privacy or ethical restrictions.

**Acknowledgments:** We would like to express my thanks to Sheng-Feng Lin from Taiwan Space Agency for supporting the preliminary investigations and the discussions of developing the ideas put forward here. Both the success of optical analysis and experiment are attributed to his invaluable advice.

**Conflicts of Interest:** The authors declare no conflict of interest.

## References

1. Uguen, G.; Luquet, P.; Chassat, F. Design and development of the 2m resolution camera for ROCSAT-2. In Proceedings of the 5th International Conference on Space Optics (ICSO 2004), Toulouse, France, 30 March–2 April 2004.
2. Lamard, J.-L.; Gaudin-Delrieu, C.; Valentini, D.; Renard, C.; Tournier, T.; Laherrere, J.-M. Design of the High Resolution Optical Instrument for the Pleiades HR Earth Observation Satellites. In Proceedings of the 5th International Conference on Space Optics (ICSO 2004), Toulouse, France, 30 March–2 April 2004.
3. CE-SAT Series, Remote Sensing Technology Center of Japan. Available online: <https://www.restec.or.jp/en/solution/product/ce-sat.html> (accessed on 10 March 2024).
4. Lin, S.-F.; Chen, C.-H.C.; Huang, Y.-K.H. Optimal F-Number of Ritchey–Chrétien Telescope Based on Tolerance Analysis of Mirror Components. *Appl. Sci.* **2020**, *10*, 5038. [[CrossRef](#)]
5. El-Maksoud, R.H.A.; Sasian, J.M. Paraxial Ghost Image Analysis. In Proceedings of the SPIE Optical Engineering + Applications, San Diego, CA, USA, 2–6 August 2009.
6. El-Maksoud, R.H.A.; Hillenbrand, M.; Sinzinger, S.; Sasian, J.M. Optical Performance of Coherent and Incoherent Imaging Systems in The Presence of Ghost Images. *Appl. Opt.* **2012**, *51*, 7134–7143. [[CrossRef](#)]
7. El-Maksoud, R.H.A. Ghost Reflections of Gaussian Beams in Anamorphic Optical Systems with An Application to Michelson Interferometer. *Appl. Opt.* **2016**, *55*, 1302–1309. [[CrossRef](#)] [[PubMed](#)]
8. El-Maksoud, R.H.A.; Sasian, J.M. Modeling and Analyzing Ghost Images for Incoherent Optical Systems. *Appl. Opt.* **2011**, *50*, 2305–2315. [[CrossRef](#)] [[PubMed](#)]
9. Grabarnik, S. Optical Design Method for Minimization of Ghost Stray Light Intensity, Optics Section, Directorate of Technical and Quality Management. *Appl. Opt.* **2015**, *54*, 3083–3089. [[CrossRef](#)] [[PubMed](#)]
10. Rogers, J.D.; Tkaczyk, T.S.; Descour, M.R. Removal of Ghost Images by Using Tilted Element Optical Systems with Polynomial Surfaces for Aberration Compensation. *Opt. Lett.* **2006**, *31*, 504–506. [[CrossRef](#)] [[PubMed](#)]
11. Younis, R.B.; Khorsheed, S.M.; Al-Dahan, Z.T. Modified Michelson Interferometer Design for Ear Measurement. *Int. J. Sci. Eng. Res.* **2018**, *6*, 36–41.
12. Hitzenberger, C.K. Low-coherence interferometry. In *Handbook of Visual Optics*; CRC Press: Boca Raton, FL, USA, 2017.

**Disclaimer/Publisher’s Note:** The statements, opinions and data contained in all publications are solely those of the individual author(s) and contributor(s) and not of MDPI and/or the editor(s). MDPI and/or the editor(s) disclaim responsibility for any injury to people or property resulting from any ideas, methods, instructions or products referred to in the content.